VUV excitation of a vibrational wavepacket in D2 measured through strong-field dissociative ionisation

VUV excitation of a vibrational wavepacket in D_2 measured through strong-field dissociative ionization

2015 New J. Phys. 17 103013

(http://iopscience.iop.org/1367-2630/17/10/103013)

New Journal of Physics
The open access journal at the forefront of physics

Deutsche Physikalische Gesellschaft DPG
IOP Institute of Physics

Published in partnership with: Deutsche Physikalische Gesellschaft and the Institute of Physics

OPEN ACCESS

RECEIVED
6 May 2015

REVISED
5 July 2015

ACCEPTED FOR PUBLICATION
14 September 2015

PUBLISHED
8 October 2015

PAPER

VUV excitation of a vibrational wavepacket in D_2 measured through strong-field dissociative ionization

A R Bainbridge[1], J Harrington[1], A Kirrander[2], C Cacho[3], E Springate[3], W A Bryan[1] and R S Minns[4]

[1] Department of Physics, College of Science, Swansea University, Singleton Park, Swansea SA2 8PP, UK
[2] School of Chemistry, University of Edinburgh, Edinburgh EH9 3FJ, UK
[3] Central Laser Facility, STFC Rutherford Appleton Laboratory, Didcot, Oxfordshire OX11 0QX, UK
[4] Chemistry, University of Southampton, Southampton, SO17 1BJ, UK

E-mail: w.a.bryan@swansea.ac.uk **and** r.s.minns@soton.ac.uk

Keywords: high harmonic generation, photoionization, vibrational wavepacket, hydrogen, chemical physics

Abstract

Femtosecond vacuum ultraviolet pulses from a monochromated high harmonic generation source excite vibrational wavepackets in the $B^1\Sigma_g^+$ state of D_2. The wavepacket motion is measured through strong field ionization into bound and dissociative ion states yielding D_2^+ and D^+ products. The time dependence of the D_2^+ and D^+ ion signals provides a sensitive fingerprint of the quantum nuclear wavepacket, due to the different ionization rates for the two channels. The experiments are modelled with excitation and ionization processes included explicitly, with the results of the model showing a very good agreement with the experimental observations. The experiment demonstrates the level of detail attainable when studying ultrafast quantum nuclear dynamics using high harmonic sources.

1. Introduction

Directly accessing highly excited electronic states of atoms and molecules with a single photon has until recently been limited to studies using synchrotron radiation sources, which provide light that is highly tunable and has narrow bandwidth. This has provided beautifully resolved spectroscopic measurements in a wide number of chemical systems highlighting, among other things, the complexities of the electronic structure of what would normally be considered relatively simple molecules [1–4]. Part of this complexity comes from the many interacting states that lie extremely close in energy. An alternative route to understanding these systems is through the study of their dynamics using time resolved spectroscopy methods [5, 6], generally requiring femtosecond to picosecond pulses of laser radiation. Since the maximum photon energy available in a conventional femtosecond laser system is limited to ~6 eV, excitation of highly excited electronic states requires the use of multiphoton excitation schemes [7, 8]. Unfortunately in many cases the strong laser fields used to achieve multiphoton excitation also drive ionization or multiple resonant excitations that limit the resolution, specificity, and population transfer into the states of interest. Sources of pulsed high-energy photons are therefore in great demand for studies of time-resolved dynamics. New technologies, such as x-ray free-electron lasers (XFELs) provide high energy light pulses with femtosecond duration that can access highly excited electronic states with a single photon. When hard x-ray energies are not required, femtosecond VUV to soft x-ray sources based on high harmonic generation (HHG) are an attractive alternative to XFELs. Light produced via HHG has the advantage over many XFEL sources in that the VUV pulse is strongly time-correlated with the driving laser pulse thus ensuring that the timing of the VUV pulse is well defined [9]. In the case of the present work, this stability has been demonstrated to be a few femtoseconds. HHG also has the ability to generate pulses of attosecond duration providing opportunities to make measurements on the sub-femtosecond timescale [10]. One issue with HHG sources is the low conversion efficiency which results in a low photon flux when compared with XFEL sources meaning the statistics of measurements made with the these sources can be very poor. The photons are also produced over a range of harmonics (energies) separated by twice the pump photon energy. Many experiments have made clever use of the many harmonics produced to study and control molecular

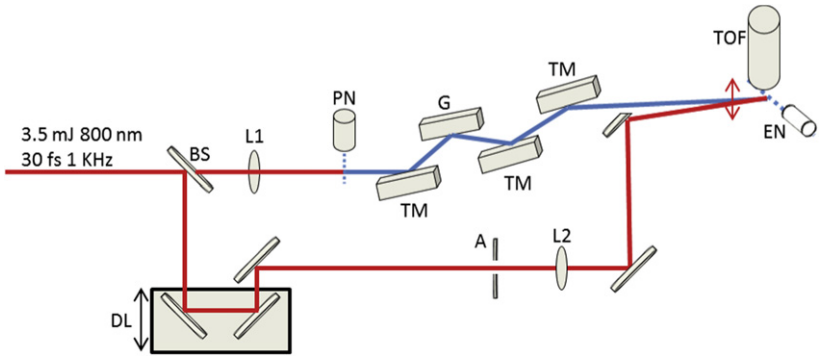

Figure 1. Schematic diagram of the experiment. A 3.5 mJ pulse is split at a beamsplitter (BS) with 1 mJ focussed into a gas jet produced by a pulsed nozzle (PN) generating high harmonics. The high harmonics are monochromated at a time preserving monochromator consisting of two toroidal mirrors (TM) and a grating (G). By tuning the grating angle the 9th harmonic is isolated and focussed into the TOFMS using a final toroidal mirror (TM). The probe beam is delayed from the pump by a mechanical translation stage delay line (DL) and is focused into the centre of the TOF where it overlaps the isolated harmonic at a small angle and intersects the beam of D_2 from the effusive nozzle (EN). To match the size of the pump beam to the probe beam an aperture is placed before the focusing optic. This also controls the intensity distribution of the pump beam at the interaction region. The double headed arrow denotes the polarization vector of the pump and probe beams, parallel to the axis of the TOFMS.

dynamics in a number of small molecular systems [11–16]. For studies of molecular dynamics originating from a single electronic state, it is often advantageous to use an isolated harmonic which provides greater control of which states are excited, and hence easier analysis and understanding of the measured dynamics. Isolating a harmonic reduces the photon flux further and often increases the duration of the pulse, reducing the temporal resolution attainable in the subsequent measurement. As a consequence, the number of experiments performed with a monochromated HHG beam as a source of pump photons for studies of gas phase molecular dynamics is comparatively small albeit growing [17–19].

In this paper we describe measurements of a vibrational wavepacket in a highly excited electronic state of D_2. The wavepacket is excited by the 9th harmonic of an 800 nm fs laser pulse which is isolated at a time preserving monochromator [20]. The resulting pulse has an energy of 14.3 eV and a duration of 25 fs. Detection of the wavepacket is via strong field ionization of the excited electronic state with an intense 800 nm (1.56 eV) laser pulse. Ionization is into both bound and dissociative ion states with the resulting atomic and molecular ions showing strong differences as a function of pump probe delay. The experiments are modelled with explicit inclusion of the pump and probe process, allowing us to explain subtle differences in the signals.

2. Experimental

The experiment is schematically represented in figure 1. An amplified femtosecond laser system (Red Dragon, KM labs) generates 30 fs duration pulses of 800 nm light with a pulse energy of 3.5 mJ. The pump and probe arms are separated at a beamsplitter with approximately 1 mJ of the 800 nm pulse being tightly focused into an Argon gas jet, generating a broad range of high harmonics. The 9th harmonic (14.3 eV) is isolated in a time preserving monochromator [20] and focused in the interaction region of a time-of-flight mass spectrometer (TOFMS) using a 1 m focal length toroidal mirror. The TOFMS has previously been employed to observe vibrational and rotational wavepackets in few cycle strong-field near infrared (NIR) pulse interactions with H_2, HD and D_2 [7, 31, 32]. Based on previous measurements the duration of the monochromated VUV pulse is approximately 25 fs [21]. The isolated harmonic is the pump pulse for the experiment and has a photon flux at the interaction region of approximately 10^7 photons per pulse as measured with a calibrated channel electron multiplier and is focused to a spot size of $\sim$140 μm. The probe is composed of the remaining 800 nm pulse not used in the generation of the high harmonics, and has duration of approximately 35 fs and controllable pulse energy. The probe is delayed with respect to the 14.3 eV pump using a mechanical translation stage and is focused in the interaction region of the TOFMS with a 1 m focal length lens. The two pulses are overlapped in time and space at the centre of the TOFMS, where they cross at a small angle of approximately 1°. A variable aperture is placed before the focusing optic of the probe beam to control the focal spot size and match this to the focal volume of the XUV beam. Spatial overlap of the VUV and IR beams is checked with a LuAG:Ce phosphorescent crystal placed at the interaction region and imaged with a CCD camera. The D_2 gas sample is delivered to the interaction region of the TOFMS using an effusive beam delivering a number density of approximately 5×10^{12} cm^{-3} where it is intersected by the pump and probe. The polarization of the pump and probe beams are parallel to the TOF axis which is in the plane perpendicular to the plane defined by the laser and

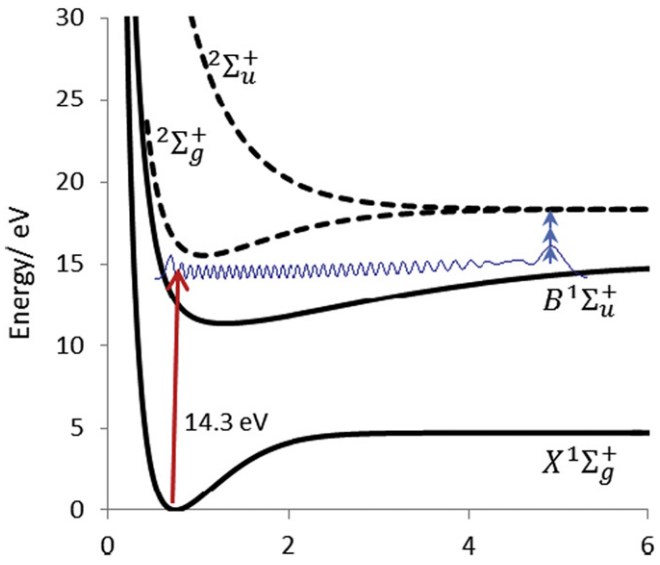

Figure 2. Potential energy curves for D2 relevant to the experiment. Single photon resonant excitation of a vibrational wavepacket in the $B^1\Sigma_u^+$ state is driven by the 9th harmonic at 14.3 eV and is centred around the $\nu = 38$ vibrational energy level. The vibrational wavepacket is the probed using a strong NIR pulse that projects the wavepacket on to the $^2\Sigma_g^+$ and $^2\Sigma_u^+$ ion states yielding either molecular or atomic ions respectively. Solid and dashed lines represent neutral and ionic electronic states respectively.

gas beams. The TOFMS allows us to separately detect the D_2^+ and D^+ ionic products produced in the experiment.

The excitation scheme is schematically represented in figure 2. The isolated 9th harmonic at 14.3 eV excites a vibrational wavepacket in the $B^1\Sigma_u^+$ state of D_2. The wavepacket is centred at the $\nu = 38$ vibrational energy level with the bandwidth of the 9th harmonic being suffficient to populate approximately 6 vibrational states in total with a Gaussian population distribution. The motion of the wavepacket is probed using a time delayed, intense NIR pulse which ionizes the $B^1\Sigma_u^+$ state population into either the $^2\Sigma_g^+$ or $^2\Sigma_u^+$ ion state producing D_2^+ and D^+ ionic products respectively.

3. Theoretical

To understand the details of the measured data each facet of the experiment is modelled, explicitly including both excitation and ionization processes. The excitation and subsequent dynamics of the wave packet can be described by solving the time-dependent Schrödinger equation [23]. Solutions are obtained in the form

$$\Psi(t) = \sum_j c_j(t) \mathrm{e}^{-\mathrm{i}E_j t/\hbar} \Psi_j, \tag{1}$$

where $\Psi(t)$ is the excited wavepacket, Ψ_j are orthonormal rovibronic wave functions and E_j are the corresponding energies. According to first-order perturbation theory, the time-dependent coefficients $c_j(t)$ are

$$c_j(t) = \mathrm{i}D_{js}\left[\frac{\mathrm{e}}{\hbar}\int_{-\infty}^{t} \mathrm{d}t' \mathrm{e}^{\mathrm{i}\omega_{js}t'} \epsilon\,(t')\right], \tag{2}$$

where D_{js} are the combined dipole transition moments and Franck–Condon factors for excitation from the initial state s to the final state j. The expression in the square brackets corresponds to the energy- and time-dependent complex excitation function with e the charge of an electron, the angular frequency $\omega_{js} = (E_j - E_s)/\hbar$ and $\epsilon(t')$ the excitation field [24, 25].

Ab-initio potential energy curves are used for the initial ground state [26] and the excited B-state [27], with dipole transition moments from [28]. The molecular mass is taken from the latest CODATA values [29]. The vibrational wave functions are calculated using a 5th order Runge–Kutta algorithm, with the orthonormality of the vibrational wave functions ensured via a Cholesky factorization, and the transition moments D_{js} calculated for $B^1\Sigma_u^+(\nu) \leftarrow X^1\Sigma_g^+(\nu = 0)$.

The calculation of tunnel ionization rates into the $^2\Sigma_g^+$ and $^2\Sigma_u^+$ states of D_2^+ by the NIR pulse is based on ADK analysis as a function of internuclear separation, where the validity of the model is defined in this case by the Keldysh parameter γ being substantially less than one. According to ADK theory the tunnelling ionization rate at a particular field is given by [22]

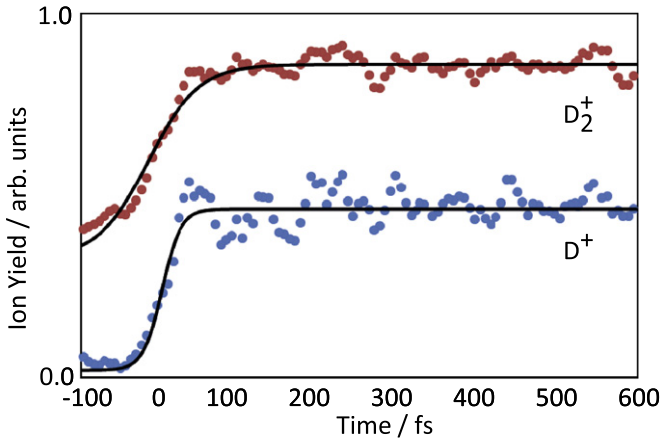

Figure 3. Measured (data points) ion yields of D_2^+ and D^+ as a function of pump probe delay fitted to equation (8) (solid lines). The lines highlight differences in the appearance time and rise time of the two signals.

$$W(E(t)) = \frac{I_p}{\hbar}|C_{n^*l^*}|^2 G_{lm}\left(\frac{4I_p}{\hbar\omega_T}\right)^{2n^*-m-l}\exp\left[{}^{-4I_p}\!/_{3\hbar\omega_T}\right], \tag{3}$$

where

$$\left|C_{n^*l^*}\right|^2 = 2^{2n^*}\left[n^*\Gamma\left(n^*+l^*+1\right)\Gamma\left(n^*-l^*\right)\right]^{-1}, \tag{4}$$

$$G_{lm} = (2l+1)(l+|m|)!\left(2^{-|m|}\right)\Big/[|m|!(l-|m|)!], \tag{5}$$

$$\omega_T = eE(t)\Big/\left[\left(2mI_p\right)^{1/2}\right], \tag{6}$$

I_p is the ionization potential, n^* is the effective principal quantum number, l is the orbital angular momentum and and m is the magnetic quantum number, $E(t)$ is the instantaneous electric field amplitude and l^* is the effective quantum number and is equal to 0 for $l \ll n$ and equals n^*-1 in all other cases. For each internuclear separation the total relative ionization rate is calculated from

$$W_{\text{Total}} = \sum_{0}^{I_{\max}}\sum_{t=-\infty}^{\infty} R(I)W(E(t)), \tag{7}$$

where $R(I)$ is the relative volume contribution for a given intensity component in the focal volume and the first sum is over all of the intensities measured by the TOFMS, the second sum then samples all field strengths for a given intensity as the sum runs over time through the laser pulse.

4. Results and discussion

In figure 3 we plot the ion yield of D_2^+ and D^+ as a function of pump probe delay, the signals are normalized and vertically offset to allow us to highlight some of the features observed. The two signals show clear differences in their overall appearance and some more subtle differences around time zero. The D_2^+ signal rises first and plateaus to an almost constant level reaching a maximum at ~40 fs. The D^+ signal then rises, with a delay of a few 10 s of femtoseconds but rises at a faster rate to also reach a maximum at ~40 fs. The D^+ signal then oscillates with a period of ~80 fs with each subsequent peak reducing in amplitude and spreading in time, indicative of vibrational motion in the anharmonic excited state potential. To obtain a more quantitative measure of the changes around time zero we first fit the signal to a generalized error function of the form

$$\text{ion yield} = \frac{A}{1+\exp\left(-\tau\left(t-t_0\right)\right)}, \tag{8}$$

where A is the amplitude of the step, t_0 is the time at which the amplitude reaches half of its maximum value, t is the time delay and τ is the time constant. From the fits, plotted as solid lines in figure 3, we observe a ~20 fs delay between the t_0 points for the D_2^+ and D^+ signals and a factor of 2.6 change in the rise-time of the fitted curves, with the $1/\tau$ value being 31 fs and 12 fs for the D_2^+ and D^+ signals respectively. The differences in the timing and the rise time, as well as the observation of much clearer and well ordered oscillations in the D^+ than in the D_2^+ signal, suggests that ionization into the bound, $^2\Sigma_g^+$, and dissociative, $^2\Sigma_u^+$, states of D_2^+ are enhanced at different

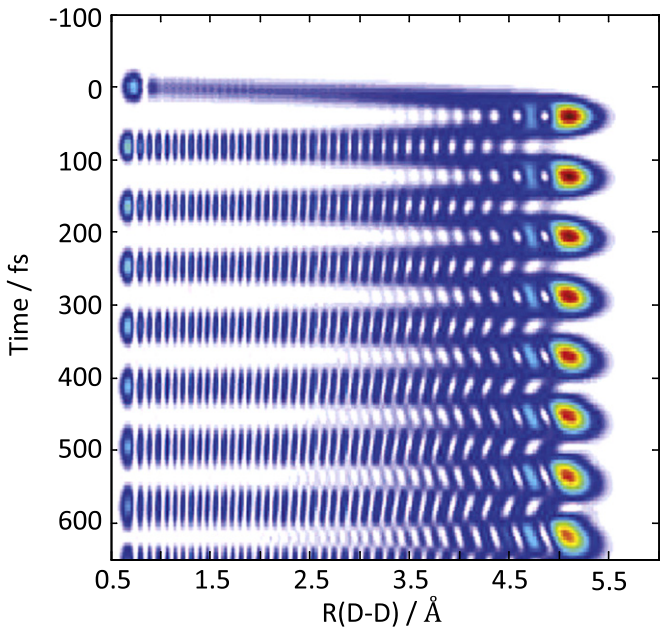

Figure 4. Calculated probability distribution of a wavepacket excited in the *B*-state of D_2 with a 25 fs duration pulse at 14.3 eV excitation energy. The wavepacket is excited at the inner turning point but does not remain there and propagates away from the inner turning point before the end of the laser pulse. The wavepacket then oscillates between the inner and outer turning points of the *B*-state potential with a period of 82 fs, gradually spreading accross the entire *B*-state potential due to the anharmonic nature of the potential.

internuclear separations, meaning that we have a sensitive probe of the wavepacket position on the *B*-state potential.

The data is modelled by first calculating the wavepacket probability distribution in the *B*-state as a function of time and position, as outlined in the theory section, with the results shown in figure 4. The theoretical beating period for the vibrational wave packet is 82 fs, matching experimental observation. Ionization of the wavepacket is driven by the non-resonant NIR pulse and is highly nonlinear and dependent on the distribution of intensities in the interaction volume measured by the TOFMS. The experimental intensity distribution of the NIR pulse is complicated by the beam aperturing before the focusing optics. The intensity distribution is calculated by solving the Huygens–Fresnel diffraction equations for a beam passing through a hard edge aperture and propagating this through the interaction region as measured by the TOFMS [30]. The calculated intensity is plotted in figure 5 (a) against the relative volume contribution as measured by the TOFMS. The intensity peaks at 5×10^{13} Wcm^{-2} but the distribution is broad with significant contributions over a wide range of intensities. It should be noted that estimating intensity distributions contains large errors. To ensure this does not create spurious results we have tested a large parameter space covering both tunnelling, multiphoton and intermediate regimes. Based on this analysis we find that the only regime that matches our experimental observations is one that is dominated by tunnelling ionization. So while we cannot be certain of the absolute intensity distribution in the interaction region as measured by the TOFMS we are confident that this lies firmly in the tunnelling regime.

Based on the calculated intensity distribution, relative ADK ionization rates are calculated, as outlined in the theoretical section, for internuclear separations between 0.4 and 6 Å, as shown in figure 5 (b). This range encompasses the inner and outer turning point which as can be seen in figure 4, are at ~0.66 and ~5 Å respectively. The large change in ionization potential over this region leads to many orders of magnitude change in the ionization rate to both ion states. This is most pronounced for ionization into the dissociative $^2\Sigma_u^+$ state where the change in ionization potential between the internuclear separations corresponding to the inner and outer turning points of the B state potential energy surface is over 19 eV. The change in ionization rate over that region is so pronounced that appreciable ionization will only occur at extended bond lengths. Conversely, for ionization into the $^2\Sigma_g^+$ state the maximum rate is seen at compressed bond lengths, however this is not as pronounced a maximum and a significant secondary maximum is also present at extended bond lengths. Appreciable ionization to the bound $^2\Sigma_g^+$ state will therefore occur at both compressed and extended bond lengths.

The calculated relative ionization rates are then multiplied by the wavepacket probability distributions for each time step in the simulation to obtain time and internuclear separation dependent relative ionization yields for each ion state, as shown in figures 6 (a) and (b). As expected, ionization into the dissociative $^2\Sigma_u^+$ ion state is peaked at extended bond lengths. As ionization into the $^2\Sigma_u^+$ state leads to dissociation, the measured D^+ signal

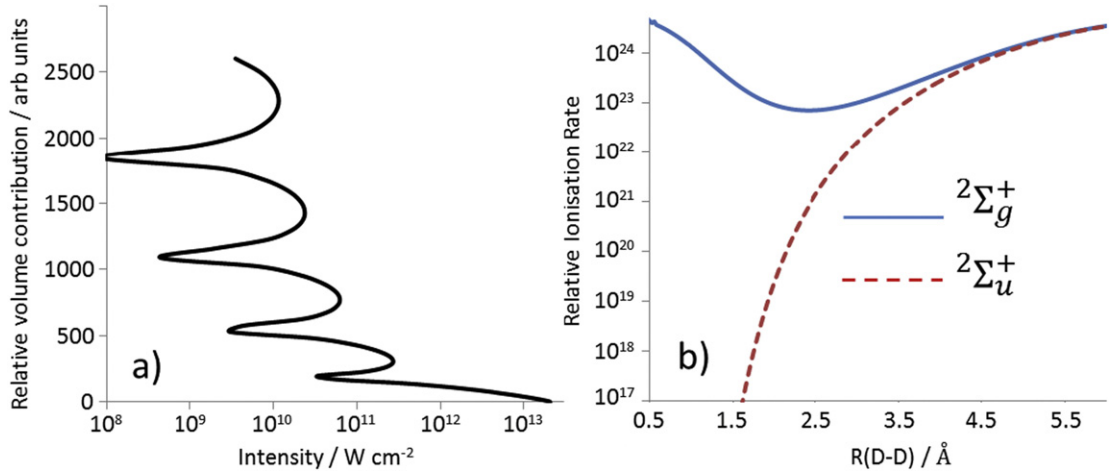

Figure 5. (a) Calculated intensity distribution in the interaction region of the TOFMS. (b) Internuclear separation dependant ionization rates based on ADK calculations for the intensity distribution given in (a).

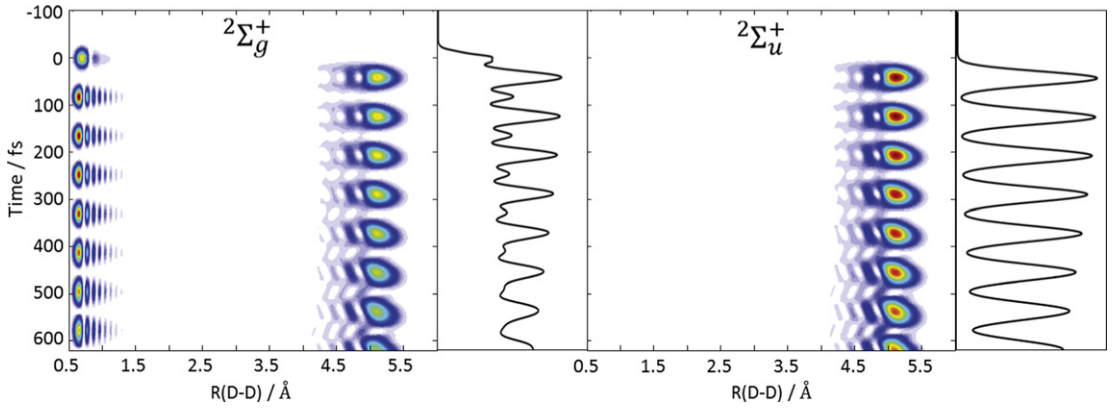

Figure 6. Contour plots of the calculated ionization probability as function of time and internuclear separation into the $^2\Sigma_g^+$ and $^2\Sigma_u^+$ ion states. The ionization rates are calculated based on the wavepacket probability distribution given in figure 4 and the relative ionization rates shown in figure 5 (b). Ionization into the $^2\Sigma_g^+$ state shows maxima at the inner and outer turning points of the *B*-state potential while ionization into the $^2\Sigma_u^+$ state only has a single maximum at the outer turning point. Line graphs to the right of the contour plots are the integrated ionization rate across all internuclear separations at a particular time delay.

provides a signature of wavepacket probability at the outer turning point of the B state potential. Ionization into the bound $^2\Sigma_g^+$ state has ionization maxima at both the inner and outer turning points. As ionization into the $^2\Sigma_g^+$ state lead to molecular ions, the D_2^+ signal will have increased yield at both the inner and outer turning points of the *B*-state potential. To the right of the contour plots in figure 6 we plot the integrated ion yield for each time step in the calculation as would be measured in the experiment if an infinitely short duration probe pulse had been used. For the $^2\Sigma_g^+$ and $^2\Sigma_u^+$ states this is equivalent to the production of D_2^+ and D^+ respectively. For ionization into the $^2\Sigma_u^+$ state, as ionization is only possible near the outer turning point the signal rise is delayed from time zero by approximately 10 fs. The first maximum in the D^+ signal is reached half a vibrational period after time zero as the wavepacket, initially localized at the inner turning point, moves to the outer turning point. Once at a maximum clear oscillations are observed every 80 fs as the molecule vibrates, oscillating between the inner turning point with reduced ionization and outer turning point where ionization is enhanced. Finally, for longer times the amplitude of each oscillation is reduced as the wavepacket spreads and the localization of the wavepacket is reduced.

The signal from ionization into the $^2\Sigma_g^+$ state is more complex. From figure 5 it is clear that the ionization rate is larger at the inner turning point than at the outer turning point however, the increased localization of the wavepacket at the outer turning point more than outweighs this affect such that maximum ionization yield is observed at the outer turning point. This gives a rather strange appearance to the D_2^+ ion yield curve. The signal starts to rise before time zero, approximately 20 fs before the D^+ signal, before starting to plateau around time zero. The plateau is caused by the balancing effects of the increased population transfer to the *B*-state from the

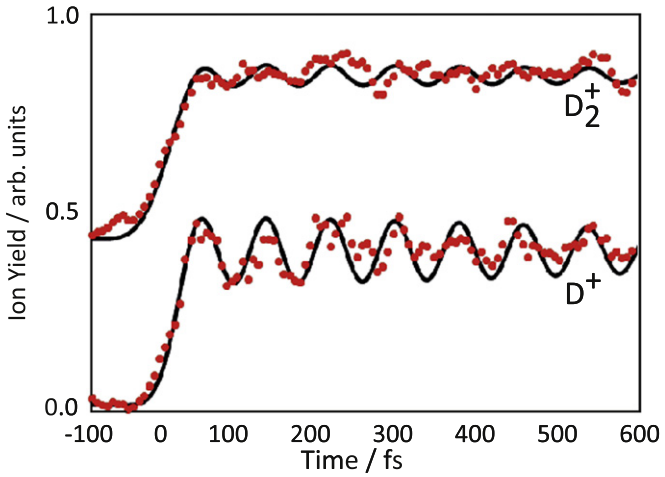

Figure 7. Experimental (solid circles) ion yields for D_2^+ and D^+ measured as a function of pump probe delay. Solid lines represent modelled ion signals based on the caluclated ionization rates shown in figure 6 convoluted with the temporal resolution of the experiment (see text for details).

pump which is still on at this time, and the motion of the wavepacket towards the centre of the *B*-state potential where ionization is reduced. The signal then rises again reaching a maximum at 40 fs as the wavepacket reaches the outer turning point. Once at a maximum the signal oscillates in phase with the D^+ signal, albeit with a greatly reduced amplitude, as the wavepacket moves between points of increased ionization yield at the outer turning point and reduced ionization yield at the inner turning point. The signal is complicated by the true minimum actually occurring when the wavepacket is localized in the centre of the *B*-state potential. As with the calculated D^+ ion signal, the oscillations become damped as the wavepacket spreads and disperses in the *B*-state potential.

To compare the calculated and experimental ion yield curves we convolute the calculated curves with a Gaussian corresponding to the experimental time resolution of ~55 fs. The results of the convolution are plotted as solid lines in figure 7, along with the experimental data, and match many of the subtle features observed in the experiment. The delay between the appearance of the D_2^+ and the D^+ signal is seen in both the experimental and calculated curves. The delay arises as the D_2^+ signal has a component from ionization at the initially excited inner turning point while D^+ is only produced when the wavepacket is at the outer turning point. Both signals also reach a maximum at 40 fs as maximum ionization occurs at the outer turning point as predicted by the calculations. The D^+ signal then oscillates with a period of 80 fs matching the classical wavepacket motion with each peak showing a reduction in peak amplitude and an increase in peak width that matches the calculation as the wavepacket disperses on the anharmonic *B*-state potential. The calculated D_2^+ signal shows similar oscillations with maxima at the same times as the D^+ signal. The effect of having maxima in ionization cross section into the bound ion state at both the inner and outer turning points reduces the amplitude of the oscillations which when combined with the blurring caused by the finite duration of the ionizing laser pulse reduces the amplitude of the observed oscillations significantly. The effect is so pronounced that the oscillations are not clearly observed in the experimental data above the noise level of the measurement. It is worth noting that the calculated signals are robust to changes in the intensity distribution calculated. We observe the same structure and period in our measurements even with extremely large changes in the maximum intensity used in the calculation.

5. Summary

This experiment illustrates the quality and resolution attainable when studying ultrafast coherent nuclear dynamics using monochromated VUV pulses from a HHG source. We excite a coherent nuclear-vibrational wavepacket in the *B*-state of D_2. The wavepacket is tracked through strong-field ionization processes that yield bound or dissociated ion fragments, both of which are monitored. As the wavepacket propagates through regions of reduced and enhanced ionization into the bound and dissociative ion states, it provides a detailed fingerprint of both the nuclear dynamics and the ionization process. Ionization into the dissociative state is strongly peaked at extended bond lengths leading to distinct oscillations in the measured and calculated D^+ signal, while ionization into the bound state is peaked at both stretched and compressed bond lengths which reduces the amplitude of the oscillation in the D_2^+ signal. The differences in ionization also lead to differences in the appearance time and how the signal rises around time zero. The D_2^+ signal has a rising edge that does not

simply correlate with excitation. The signal rises as increased population is transferred into the *B*-state from the pump, however, maximum ionization occurs at the outer turning point such that the signal continues to rise as the wavepacket moves towards the outer turning point. This gives the appearance of a slowly rising signal when compared with D^+ which is only produced at the outer turning point. Our analysis highlights the need to explicitly include both excitation and probe processes in the modelling of apparently simple dynamics to unravel the subtleties of the measured experimental signals.

Acknowledgments

The authors gratefully acknowledge support from the STFC for funding access to the Artemis laser facility (application number 111012). RSM would like to thank the Royal Society for Fellowship funding (UF100047). RSM and AK would like to thank the Leverhulme trust for research funding (RPG-2013-365). ARB gratefully acknowledges support from EPSRC. We thank Phil Rice for technical assistance. AK would like to acknowledge grant FP7-PEOPLE-2013-CIG-NEWLIGHT from the European Union. Information of how to obtain data and materials presented in this publication can be obtained from http://eprints.soton.ac.uk/id/eprint/382045.

References

[1] Glass-Maujean M *et al* 2010 *Phys. Rev. Lett.* **104** 183002
[2] Glass-Maujean M *et al* 2010 *Phys. Rev.* A **82**
[3] Glass-Maujean M *et al* 2011 *J. Chem. Phys.* **135** 144302
[4] Gilkison A T, Viteri C R and Grant E R 2004 *Phys. Rev. Lett.* **92** 173005
[5] Minns R S *et al* 2003 *J. Chem. Phys.* **119** 5842
[6] Smith R A L *et al* 2003 *J. Chem. Phys.* **119** 3085
[7] Bryan W A *et al* 2011 *Phys. Rev.* A **83** 021406(R)
[8] Pisharody S N and Jones R R 2004 *Science* **303** 813
[9] Ranitovic P *et al* 2014 *PNAS* **111** 912
[10] Sansone G *et al* 2010 *Nature* **465** 763
[11] Zhou X *et al* 2012 *Nat. Phys.* **8** 232
[12] Kelkensberg F *et al* 2011 *Phys. Rev. Lett.* **107** 043002
[13] Furukawa Y *et al* 2010 *Phys. Rev.* A **82** 013421
[14] Okino T *et al* 2014 *J. Phys. B.: At. Mol. Opt. Phys.* **47** 124007
[15] Singh K P *et al* 2010 *Phys. Rev. Lett.* **104** 023001
[16] Carpeggiani P A *et al* 2014 *Phys. Rev.* A **89** 023420
[17] Cao W *et al* 2015 *Phys. Rev. Lett.* **114** 113001
[18] Strasser D *et al* 2006 *Phys. Rev.* A **73** 021805(R)
[19] Doughty B *et al* 2012 *J. Chem. Phys.* **136** 214303
[20] Frassetto F *et al* 2011 *Opt. Express* **19** 19169
[21] Bryan W A *et al* 2012 *New J. Phys.* **14** 013057
[22] Bransden B H and Joachain C J 2003 *Physics of Atoms and Molecules* 2nd edn (Englewood Cliffs, NJ: Prentice-Hall)
[23] Kirrander A, Fielding H H and Jungen Ch 2007 *J. Chem. Phys.* **127** 164301
[24] Kirrander A, Jungen C and Fielding H H 2010 *Phys. Chem. Chem. Phys.* **12** 8948
[25] Kirrander A, Jungen Ch and Fielding H H 2008 *J. Phys. B.: At. Mol. Opt. Phys.* **41** 074022
[26] Wolniewicz L 1995 *J. Chem. Phys.* **103** 1792
[27] Staszewska G and Wolniewicz L 2002 *J. Mol. Spectrosc.* **212** 208
[28] Wolniewicz L and Staszewska G 2003 *J. Mol. Spectrosc.* **217** 181
[29] Mohr Peter J, Taylor Barry N and David B 2012 *Newell Rev. Mod. Phys.* **84** 1527
[30] Nemeth G R A J and Bryan W A 2011 *J. Mod. Opt.* **58** 1214
[31] Calvert C R *et al* 2010 *Phys. Rep.* **491** 1–28
[32] Bryan W A *et al* 2011 *Faraday Discuss.* **153** 343–60